Spatial Mapping of Remote Photoplethysmography Quality in the Anterior Neck for Contactless Heart Rate Monitoring

Mohammad Muntasir Rahman[1], Amirtahà Taebi[1]

[1] Lehigh University, Bethlehem, PA, USA

Abstract

Remote photoplethysmography (rPPG) has traditionally relied on facial videos for contactless cardiovascular monitoring; however, the anterior neck presents a promising alternative due to the superficial proximity of the carotid arteries. Despite this advantage, rPPG signals in the neck region are often affected by spatial variability in signal quality. This paper proposes a systematic framework to characterize the spatial distribution of rPPG signals across the neck. By partitioning the neck region of interest (ROI) into a 10×20 *grid, we independently extract rPPG signals from 200 discrete spatial cells. A composite quality metric,* $\mathcal{S}$*, is developed by combining temporally normalized signal energy with spectral signal-to-noise ratio (SNR). Results reveal pronounced spatial heterogeneity and subject-specific variability in signal quality. Bland-Altman analysis demonstrates that combined rPPG signal from the cells in the upper-quartile composite quality (*$\mathcal{S} > Q3$*) regions achieve high agreement with gold-standard ECG (mean bias: 1.09 bpm; limits of agreement:* -6.83 *to* 9.01 *bpm), whereas those within the lower-quartile* $\mathcal{S}$ *(*$\mathcal{S} < Q1$*) regions exhibit a dramatic degradation in accuracy (limits of agreement:* -26.09 *to* 28.62 *bpm). These findings underline the necessity of spatially adaptive signal selection and provide motivations for subject-specific ROI optimization in neck-based rPPG.*

1. Introduction

Remote photoplethysmography (rPPG) has emerged as a powerful technique for contactless monitoring of cardiovascular activity by analyzing subtle color variations in skin regions captured by standard cameras. Unlike most traditional contact-based methods, rPPG enables unobtrusive and scalable physiological sensing, making it suitable for telemedicine, affective computing, and long-term monitoring applications [1–3]. Most existing rPPG studies focus on facial regions due to their relatively stable illumination conditions and rich superficial vascularization [4]. However, facial imagery inherently contains identifiable biometric features, increasing the subject re-identification risk even in anonymized datasets [5]. To address this challenge, recent efforts have explored alternative anatomical regions that may enable privacy-preserving rPPG measurements. The anterior neck is a promising candidate due to its proximity to major blood vessels, including the carotid artery and jugular vein, while containing fewer identifiable visual features compared to the face.

Early studies demonstrated that pulsatile activity in the neck can be captured using conventional imaging systems [6]. Subsequent work refined these approaches by analyzing localized skin regions to extract vascular signals, including jugular venous pulse waveforms using near-infrared imaging [7]. Other studies investigated motion-based approaches, capturing carotid-induced skin displacements using RGB cameras [8]. More recently, high-resolution and high-speed imaging have been used to localize pulsatile activity on specific regions of the neck using fine spatial grids [9]. Despite these advances, most prior studies focus on lateral or oblique views of the neck and often target specific vascular structures. In contrast, the spatial characteristics of rPPG signals across the anterior neck region remain poorly understood. Variations in vascular anatomy, skin properties, motion artifacts, and illumination can lead to heterogeneous signal quality across different regions on the neck. In addition, anterior neck presents additional challenges, including motion artifacts from swallowing and the coexistence of different vascular sources. Understanding this spatial variability is critical for improving signal extraction, optimizing region-of-interest (ROI) selection, and enhancing the robustness of rPPG-based systems.

Building upon our prior neck-based rPPG feasibility studies [10, 11], this paper provides a comprehensive characterization of the spatial signal quality distribution across the anterior neck. Our primary contribution is a grid-based framework that generates a composite signal quality map by integrating temporal signal energy with spectral signal-to-noise ratio (SNR). We partition the ROI into 200 cells, independently extracting and analyzing signals from each cell. This allows for analyzing the ROI for regions with high physiological salience.

2. Methodology

2.1. Data Acquisition and Protocol

An initial cohort of 35 adult participants (11 female) was recruited under protocols approved by the institutional review boards of Lehigh University and Mississippi State University, and all participants provided informed consent. This study focuses on a subset (Subjects 20–35) providing simultaneous ECG and PPG data. Data were collected during two 15-second respiratory breath-hold conditions at the end of inhalation (BHEI) and exhalation (BHEE). Following data quality assessment, Subject 30 was excluded due to hardware issue, and the BHEI recording from Subject 25 was removed due to synchronization failure, resulting in 15 participants (4 female) for the final analysis.

Participants were in a supine posture and instructed to remain still to minimize motion artifacts. Video recordings were acquired using an iPhone 13 Pro (Apple Inc., USA) at 60 fps with a spatial resolution of 3840×2160 pixels. The device was mounted on a fixed holder, and recording was initiated using Bluetooth camera shutter to avoid camera vibrations. Reference physiological signals were collected concurrently at 5 kHz using a fingertip pulse oximeter (P02-200, iWorx Systems Inc., USA) and a single-lead ECG system (iWire-B3G, iWorx Systems Inc., USA). To ensure temporal alignment between video and physiological recordings, an audio-based synchronization strategy was employed. Distinct acoustic markers generated at the beginning and end of each recording were captured by both systems and used for post hoc alignment.

2.2. ROI Definition and Tracking

To standardize analysis across subjects, the ROI was defined using bilateral nipple landmarks and the left and right neck-shoulder junctions in the first video frame, as described in [11]. To correct for body orientation, frames were rotated to horizontally align the line connecting the nipples, ensuring a vertical orientation of the sternum in all videos. The ROI width and height were defined as 90% of the neck width and 20% of the vertical distance between the neck and nipples. To account for minor subject movements during recording, the ROI was tracked across frames using normalized cross-correlation template matching.

2.3. Grid-Based rPPG Signal Extraction

We partitioned the ROI into a 10×20 grid rather than averaging rPPG over the entire neck region, yielding 200 independent spatial cells for localized rPPG signal analysis. For each cell $C_{i,j}$, the average green channel intensity $G_{i,j}(t)$ was extracted as the primary rPPG source due to its superior SNR in the hemoglobin absorption spectrum [1]. The raw signal for each cell was defined as $G_{i,j}(t) = 1/N_{i,j} \sum_{(x,y)\in C_{i,j}} G(x, y, t)$, where $N_{i,j}$ denotes the number of pixels in cell $C_{i,j}$.

Signals were detrended and bandpass filtered (0.6–4.0 Hz) using a zero-phase Butterworth filter. To mitigate filtering edge artifacts, symmetric padding was applied prior to filtering and removed afterward. Because reflection-based rPPG signals can have inverted polarity relative to transmission-based PPG, signal polarity was adjusted to be consistent with the reference fingertip PPG signals.

2.4. rPPG Signal Energy Calculation

To quantify the spatial distribution of rPPG signals, noisy signal intervals caused by motion, illumination changes, or swallowing were first identified and excluded. To ensure temporal consistency and avoid fragmentation effects, longest clean segment was selected for each cell, denoted as $T_{i,j}^{\text{clean}}$. The energy of each cell was defined as $E_{i,j} = \sum_{t\in T_{i,j}^{\text{clean}}} x_{i,j}^2(t)$, where $x_{i,j}(t)$ denotes the preprocessed rPPG signal. To account for variations in segment duration, the energy was normalized by the length of the selected segment, yielding an energy-per-second measure $E_{i,j}^{\text{sec}} = E_{i,j}/|T_{i,j}^{\text{clean}}|$, where $|T_{i,j}^{\text{clean}}|$ denotes the duration (in seconds) of the segment.

2.5. Spectral SNR Estimation

Signal quality was also quantified using a spectral SNR computed on the same clean segment. The rPPG signal was temporally aligned with the reference PPG using cross-correlation-based lag estimation. Following the De Haan framework [3], power spectral density was estimated using Welch's method with an adaptive Hamming window. The SNR was defined as the ratio of the power within the cardiac fundamental and first harmonic to the remaining power within the physiological band (0.6–4.0 Hz):

$$\text{SNR}_{i,j} = 10 \log \left(\frac{\sum_{f\in\Omega} P_{\text{rppg}}(f)\cdot\Delta f}{\sum_{f\in B} P_{\text{rppg}}(f)\cdot\Delta f - \sum_{f\in\Omega} P_{\text{rppg}}(f)\cdot\Delta f} \right) \tag{1}$$

where Ω represents the cardiac bins (ground-truth $f_{\text{HR}} \pm 0.1$ Hz and $2f_{\text{HR}} \pm 0.1$ Hz) and B represents the total physiological bandwidth [3].

2.6. Composite Spatial Quality Metric

To enable inter-subject comparison, the energy and SNR values were normalized on a per-subject basis using min–max scaling. A composite quality metric was then calculated as $\mathcal{S}_{i,j} = E_{i,j}^{\text{norm}} \cdot \text{SNR}_{\text{i,j}}^{\text{norm}}$. The resulting $\mathcal{S}$ values were projected onto their corresponding spatial grid locations to generate rPPG signal quality maps across the neck.

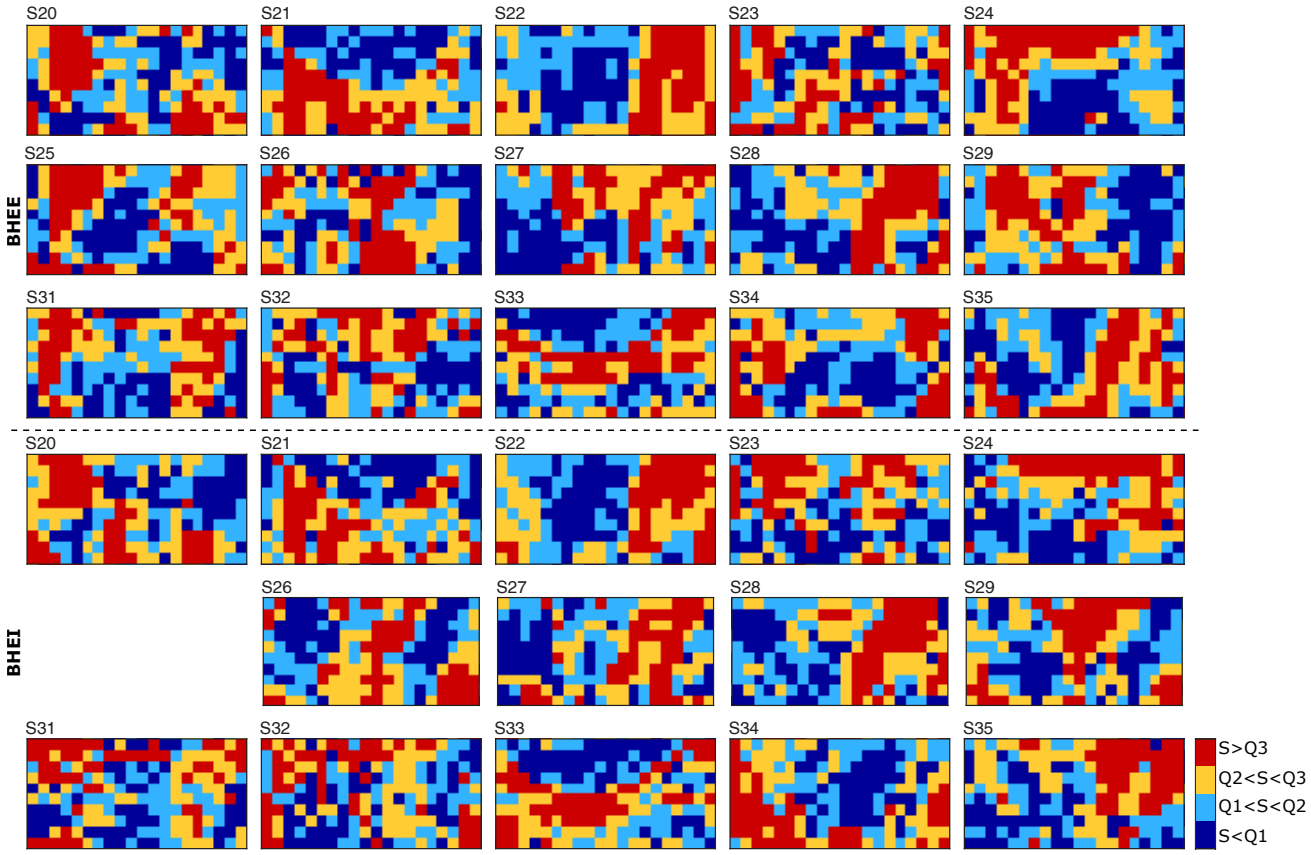

Figure 1. Spatial distribution of the composite quality metric, $\mathcal{S}$, visualized on a 10×20 grid for 15 participants under two breath-hold conditions: end-exhalation (BHEE, top) and end-inhalation (BHEI, bottom). To enable inter-subject comparison, maps are normalized per subject and discretized using interquartile thresholds. Color coding indicates relative signal quality: dark blue ($\mathcal{S} < Q1$), light blue ($Q1 < \mathcal{S} < Q2$), yellow ($Q2 < \mathcal{S} < Q3$), and red ($\mathcal{S} > Q3$).

3. Results and Discussion

3.1. Spatial Distribution of rPPG Quality

The proposed composite quality metric $\mathcal{S}$ was used to generate subject-specific spatial maps over the 10×20 grid (Figure 1). To enhance interpretability, each map was discretized using interquartile range (IQR)-based thresholds. Specifically, grid cells were categorized into four groups: $\mathcal{S} < Q1$, $Q1 < \mathcal{S} < Q2$, $Q2 < \mathcal{S} < Q3$, and $\mathcal{S} > Q3$, where $Q1$, $Q2$, and $Q3$ were the first quartile, median, and third quartile.

The resulting maps revealed spatial heterogeneity in rPPG signal quality across the subjects. Notably, regions with values of $\mathcal{S}$ exceeding $Q3$ typically formed spatially localized clusters, indicating the presence of subject-specific high-quality regions within the neck area. These findings suggest that rPPG signal quality is not uniformly distributed and that certain subject-specific anatomical regions may provide more reliable physiological information.

3.2. rPPG-Based Heart Rate Accuracy

To assess the practical impact of spatial variability on estimating cardiac metrics, combined rPPG signals were reconstructed for regions with high and low $\mathcal{S}$ scores. These regions include: (i) the upper-quartile regions defined as grid cells with values of $\mathcal{S}$ greater than $Q3$, and (ii) lower-quartile regions defined as cells with values of $\mathcal{S}$ below $Q1$. For each region, a representative rPPG signal was computed which was used to estimate heart rate (HR).

The accuracy of rPPG-based HR estimation was evaluated against ECG-derived ground truth using Bland-Altman analysis, as shown in Figure 2. The results demonstrate a clear difference in performance between the two regions. For the upper-quartile regions ($\mathcal{S} > Q3$), the mean bias was 1.09 bpm, with limits of agreement ranging from -6.83 bpm to 9.01 bpm. These relatively narrow limits indicate strong agreement and low variability in HR estimation. In contrast, lower-quartile regions ($\mathcal{S} < Q1$) yielded a similar mean bias of 1.27 bpm but exhibited substantially wider limits of agreement, ranging from -26.09

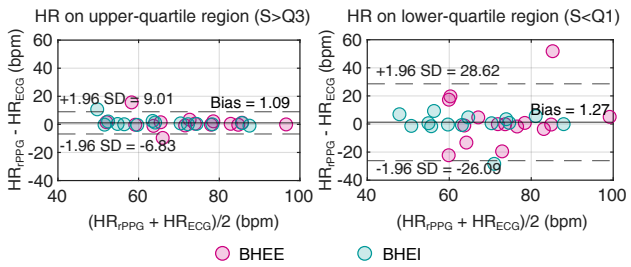

Figure 2. Bland-Altman analysis of rPPG-based heart rates (HRs) estimated from the $\mathcal{S} > Q3$ (upper-quartile) and $\mathcal{S} < Q1$ (lower-quartile) regions against the ground-truth ECG-derived HR, evaluated across all subjects.

bpm to 28.62 bpm. This large spread reflects significant variability and reduced reliability in HR estimation when signals are extracted from lower-quartile $\mathcal{S}$ regions.

3.3. Need for Subject-Specific Analysis

The results highlight that the proposed composite metric effectively identifies spatial regions that are most informative for rPPG-based physiological monitoring. By integrating signal energy and SNR into a unified metric, the proposed approach jointly captures signal amplitude and physiological consistency. Although both lower- and upper-quartile regions exhibit comparable mean bias, the variance of estimation error differs markedly. This indicates that the limitation of neck regions with lower quality rPPG signals is not systematic bias but instability and noise. The observed subject-specific variability in neck locations with higher quality rPPG signals suggests that optimal sensing regions differ across individuals. This finding underscores the limitation of conventional approaches that rely on global ROI averaging and highlights the importance of spatially adaptive signal selection. Overall, the results demonstrate that selecting high-quality regions significantly improves the reliability of rPPG-derived HR estimation.

4. Conclusion

We presented a grid-based framework for analyzing the spatial distribution of rPPG signals on the anterior neck based on a composite quality metric $\mathcal{S}$ that integrates temporal energy and spectral SNR. Experimental results demonstrate that anterior neck regions with a higher $\mathcal{S}$ ($> Q3$) yield significantly more reliable heart rate estimates, with substantially reduced variability compared to those estimated from regions with a $\mathcal{S} < Q1$. The findings further reveal that rPPG signal quality is spatially heterogeneous and subject-specific, emphasizing the need for localized signal selection rather than global averaging.

Acknowledgments

This work was supported by the U.S. National Science Foundation (Grant No. 2340020 and 2618456).

References

[1] Verkruysse W, Svaasand LO, Nelson JS. Remote plethysmographic imaging using ambient light. Optics express 2008;16(26):21434–21445.

[2] Poh MZ, McDuff DJ, Picard RW. Non-contact, automated cardiac pulse measurements using video imaging and blind source separation. Optics express 2010;18(10):10762–10774.

[3] De Haan G, Jeanne V. Robust pulse rate from chrominance-based rPPG. IEEE transactions on biomedical engineering 2013;60(10):2878–2886.

[4] Wang W, Den Brinker AC, Stuijk S, De Haan G. Algorithmic principles of remote PPG. IEEE Transactions on Biomedical Engineering 2017;64(7):1479–1491.

[5] Wang W, Den Brinker AC, De Haan G. Single-element remote-ppg. IEEE Transactions on Biomedical Engineering 2018;66(7):2032–2043.

[6] Dang TT, Huynh C, Dinh A, Tran K. Recognizing area of pulsations on the neck via video camera systems. In 2015 International Conference on Advanced Technologies for Communications (ATC). 2015; 139–144.

[7] Amelard R, Hughson RL, Greaves DK, Pfisterer KJ, Leung J, Clausi DA, Wong A. Non-contact hemodynamic imaging reveals the jugular venous pulse waveform. Scientific reports 2017;7(1):40150.

[8] Moco AV, Mondragon L, Wang W, Stuijk S, De Haan G. Camera-based assessment of arterial stiffness and wave reflection parameters from neck micro-motion. Physiological measurement 2017;38(8):1576.

[9] Cao M, Saiko G, Douplik A. Remote physiological monitoring of neck blood vessels with a high-speed camera. Advanced Optical Technologies 2025;14:1536415.

[10] Rahman MM, Taebi A. Contactless heart rate and heart rate variability estimation from neck videos. In 2025 47th Annual International Conference of the IEEE Engineering in Medicine and Biology Society (EMBC). 2025; .

[11] Rahman MM, Taebi A. Heart rate monitoring from smartphone neck videos using remote photoplethysmography. Journal of Engineering and Science in Medical Diagnostics and Therapy 2026;9(2):021009.

Address for correspondence:

Amirtahà Taebi
Department of Bioengineering, Lehigh University, Bethlehem, PA 18015, USA
e-mail: amirtaha@lehigh.edu